Nano Energy 38 (2017) 12–18

Contents lists available at ScienceDirect

Nano Energy

journal homepage: www.elsevier.com/locate/nanoen

Communication

Double-oxide sulfur host for advanced lithium-sulfur batteries

Weijiang Xue[a,b], Qing-Bo Yan[b,c], Guiyin Xu[b], Liumin Suo[b], Yuming Chen[b], Chao Wang[b], Chang-An Wang[a,*], Ju Li[b,*]

[a] State Key Lab of New Ceramics and Fine Processing, School of Materials Science and Engineering, Tsinghua University, Beijing 100084, PR China
[b] Department of Nuclear Science and Engineering and Department of Materials Science and Engineering, Massachusetts Institute of Technology, Cambridge, MA 02139, USA
[c] College of Materials Science and Opto-Electronic Technology, University of Chinese Academy of Science, Beijing 100049, PR China

ARTICLE INFO

Keywords:
Polysulfides adsorption
Double-oxide sulfur host
Sulfur cathode
Secondary particle

ABSTRACT

Although lithium-sulfur batteries show fascinating potential for high-capacity energy storage, their practical applications are hindered by the fast capacity decay and low sulfur utilization at high sulfur loading. Herein we report an efficient sulfur host based on two oxides, in which SiO_2 hollow spheres with radial meso-channels are covered by a thin TiO_2 coating. SiO_2 spheres not only yield high sulfur loading as high as 80 wt% but also possess strong lithium polysulfides (LiPS) adsorption capability. The thin TiO_2 coating can effectively prevent the LiPS outward diffusion, giving rise to a long-term stability. Meanwhile, the oxide-supported carbon from the carbonization of surfactants enables good electrical conductivity to facilitate electron access and improve sulfur utilization. Experimental and theoretical studies show the strong adsorption of LiPS by SiO_2. Benefitting from the unique structural and compositional advantages, we achieve a high sulfur loading up to 80 wt% with ~65.5% and 33% capacity retentions over 500 and 1000 cycles when tested at 0.5 C and 1 C, respectively.

1. Introduction

Lithium-sulfur (Li-S) batteries have received considerable attention because of the high theoretical specific energy of 2567 Wh/kg and specific capacity of 1675 mAh/g delivered by the element sulfur, which is characterized by its natural abundance, low cost and non-toxicity [1]. Unfortunately, several major issues have to be addressed for realizing the practical application of Li-S batteries: i) The full utilization of sulfur is hindered by the intrinsically very low electronic conductivity of both sulfur (5×10^{-30} S cm^{-1}) and its discharge product lithium sulfide (Li_2S); ii) Sulfur undergoes a large volume expansion (~80%) upon full lithiation to Li_2S, which can cause pulverization and structural damage at the electrode level. iii) The intermediate long chain LiPS (Li_2S_x, $4\leq x\leq 8$) species are very soluble in liquid electrolytes, "shuttling" between lithium metal anode and sulfur cathode resulting in fast capacity degradation and poor Coulombic efficiency.

To overcome the above-mentioned problems, a tremendous amount of work [2–7] has been done especially since Nazar et al. achieved a great breakthrough in 2009 [8]. The typical strategy is to incorporate various carbon-based materials into sulfur cathodes, including carbon nanotubes [9,10], graphene [11–13], carbon nanofibers [14,15] and so on. Although carbon-based materials are very effective in improving the conductivity and facilitating sulfur utilization, their nonpolar nature shows only limited affinity for LiPS adsorption. To further modulate the LiPS adsorption capability and hence mitigate the "shuttle effect", metal oxides [16] have drawn extensive attention recently in view of their strong polar-polar [2] chemical interaction with LiPS. So far, a variety of metal oxides, such as MnO_2 [17–19], V_2O_5 [20,21], TiO_2 [22] and Si/SiO_2 [23], have been explored as effective sulfur hosts for Li-S batteries.

However, the sulfur loading in these oxides is usually limited, which correspondingly makes it difficult to achieve high energy density of Li-S batteries. So far, there have been only a few reports [20,24] demonstrating high sulfur loading above 70 wt% with only single oxide as the sulfur host material. Furthermore, the intrinsically poor electrical conductivity of these oxides can further decrease the electrochemical performance. Therefore, it is still a great challenge to design and synthesize an advanced metal oxide nanostructure as a more efficient sulfur host, which is expected to exhibit very strong LiPS adsorption capability, high sulfur loading and good conductivity at the same time.

SiO_2 has theoretical density 2.65 g/cm^3 and is among the lightest of solid oxides. It can provide mesoporous host surface [25–28] and mechanical support for conductive carbon to mitigate the negative impact of the large volume change (~80%) between S↔Li_2S that may otherwise fracture the conductive network. TiO_2 is known to provide trapping and electrocatalysis for LiPS [29], but it is heavier (4.23 g/

* Corresponding authors.
E-mail addresses: wangca@mail.tsinghua.edu.cn (C.-A. Wang), liju@mit.edu (J. Li).

http://dx.doi.org/10.1016/j.nanoen.2017.05.041
Received 28 March 2017; Received in revised form 30 April 2017; Accepted 17 May 2017
Available online 17 May 2017

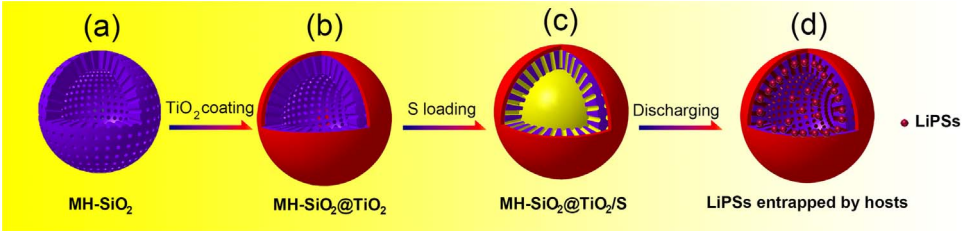

Fig. 1. Schematic illustration of the synthesis strategy of MH-SiO_2@TiO_2 host materials.

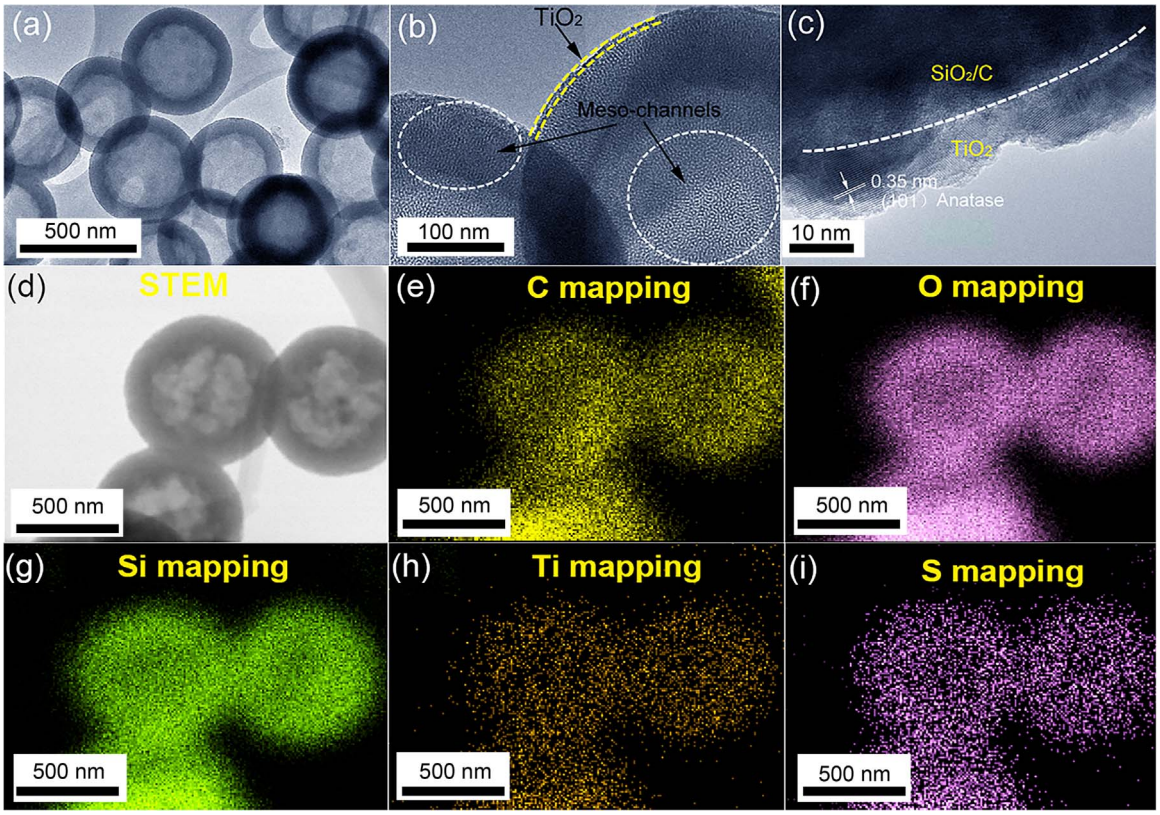

Fig. 2. Characterization of the microstructure and elemental distribution of MH-SiO_2@TiO_2 and MH-SiO_2@TiO_2/S composites. (a)~(c) TEM and HRTEM images of MH-SiO_2@TiO_2; (d) STEM image of MH-SiO_2@TiO_2/S composites; (e)~(i) EDS elemental mapping images of C, O, Si, Ti, S.

cm^3), and therefore it is suggested to be applied as a nano-coating on SiO_2 spheres to alleviate the weight effect. An additional benefit is that nano TiO_2 becomes conductive to Li ions and electrons when its thickness is less than 20 nm [30]. Herein we design and synthesize an efficient double-oxide host in which SiO_2 hollow spheres with radial meso-channels are covered by a thin TiO_2 coating (MH-SiO_2@TiO_2). The advantages of such host are: (i) MH-SiO_2 spheres not only yield high sulfur loading as high as 80 wt% but also possess strong LiPS adsorption capability [23,31–33]. Meanwhile, the thin TiO_2 coating can effectively prevent the LiPS outward diffusion, giving rise to a better cycle stability. (ii) The carbonization of surfactants used in the synthesis process at high temperature can produce carbonaceous materials in the MH-SiO_2@TiO_2, enabling good electrical conductivity for facilitating the electron access and hence improving sulfur utilization. In some sense, we are designing a "composite secondary particle" for the cathode. Furthermore, first-principles calculations and X-ray photoelectron spectroscopy (XPS) results characterize the bonding mechanism of LiPS with our double oxides. To our knowledge, no systematic investigation has been performed on the detailed bonding mechanism between LiPS and SiO_2. As a result, the MH-SiO_2@TiO_2/S composite cathodes deliver excellent cycling performances at both 0.5 C and 1 C.

2. Results and discussion

The synthesis of MH-SiO_2@TiO_2 is illustrated in Fig. 1. Uniform SiO_2 hollow spheres with meso-channels shown in Fig. 1(a) were first prepared via a simple and facile self-assembly method using structure-directing agents CTAB. As shown in Fig. 1(b), MH-SiO_2 spheres were then covered by coating a thin layer composed of TiO_2 nanoparticles in the presence of surfactant. Subsequent heat-treatment under Ar at 800 °C resulted in the densification, crystallization and more importantly, the carbonization of surfactants to produce carbons to improve the conductivity. Unless stated otherwise, the sulfur host material is always the MH-SiO_2@TiO_2 annealed at 800 °C for 2 h under Ar in the following paragraphs. Next, commercial sulfur was incorporated into the MH-SiO_2@TiO_2 host via a conventional melt-diffusion method at 155 °C, as demonstrated in Fig. 1(c). The design strategy is to enable LiPS stemming from the reaction between lithium ion and sulfur to be anchored to both the TiO_2 shell and SiO_2/C meso-channels during the discharging process in Fig. 1(d).

The as-prepared silica spheres are relatively monodisperse (~450 nm diameter) [34]. The hollow structures can also be clearly identified from SEM image of MH-SiO_2 shown in Fig. S1(a). By controlling the incubation time in hot water, the shell thickness can be adjusted, as demonstrated by TEM micrographs of samples with

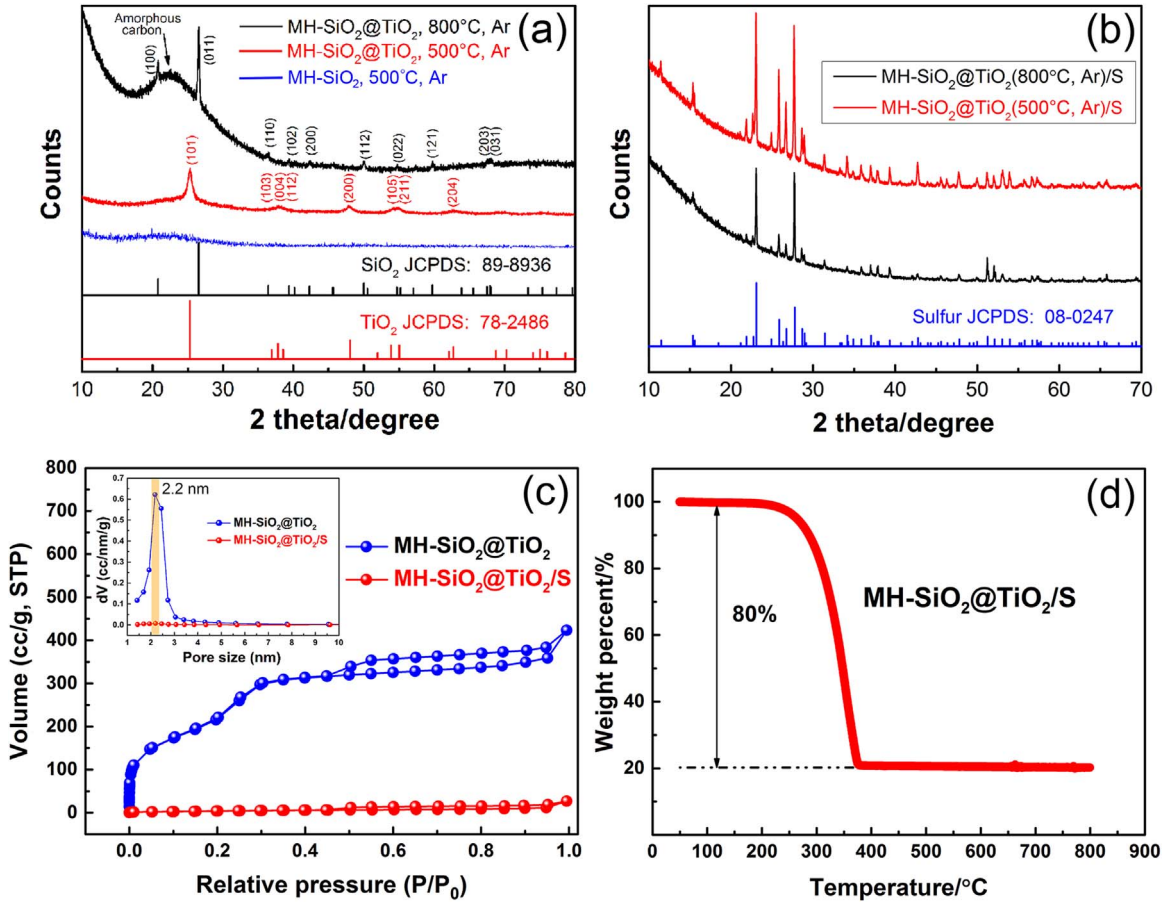

Fig. 3. Characterization of MH-SiO_2@TiO_2 and MH-SiO_2@TiO_2/S composites and other control samples. (a) XRD patterns of MH-SiO_2, MH-SiO_2@TiO_2 heat-treated at 500 °C and 800 °C; (b) XRD patterns of samples in (a) after sulfur infiltration by melt-diffusion method at 155 °C; (c) Nitrogen adsorption-desorption isotherms and pore size distribution curves of MH-SiO_2@TiO_2 samples before and after sulfur infiltration; (d) Thermogravimetric analysis (TGA) from room temperature to 800 °C at a heating rate of 10 °C/min under N_2 atmosphere to determine the sulfur content.

24 h, 48 h and 72 h incubation time in Fig. S2. In the following experiments, we select the sample with ~80 nm shell thickness (48 h incubation time) because it can balance optimization between the specific surface area and LiPS confining capability. After coating MH-SiO_2 with a thin layer of TiO_2 by the hydrolysis of tetrabutylorthotitanate (TBOT) in the presence of hydroxypropyl cellulose (HPC), the MH-SiO_2@TiO_2 samples still well maintain the spherical shape with smooth surfaces (Fig. S1b). TEM micrographs in Fig. S3 obviously present continuous and uniform TiO_2 coatings on SiO_2 spheres. In order to further characterize the morphology, TEM and HRTEM observations were conducted on the MH-SiO_2@TiO_2 samples after heat-treatment, as shown in Fig. 2(a)~(c). Continuous meso-channels throughout the shell can be observed from the high-magnification TEM image in Fig. 2(b), suggesting that the electrolyte can be readily accessible to even the core part of the material. Such meso-channels with highly polar surface have favorable LiPS adsorption capability similar to the mesoporous silica SBA-15 in a previous report [33]. In addition, the thickness of the TiO_2 coating is estimated to be about 10 nm from the HRTEM image in Fig. 2(c). The lattice fringes of the TiO_2 nanocrystals correspond to the (101) planes of anatase TiO_2, according to the standard PDF card JCPDS No. 78-2486. After incorporating sulfur into MH-SiO_2@TiO_2 at 155 °C for 12 h, well retained spherical morphology can be observed clearly from the STEM image in Fig. 2(d). To further reveal the elements distribution of MH-SiO_2@TiO_2/S composite, the elemental mapping by EDX was performed (Fig. 2(e)~(i)), demonstrating that sulfur has been uniformly confined within the hosts. Furthermore, the homogeneous distribution of carbon throughout the whole microstructure can greatly improve the electronic conductivity of SiO_2 and TiO_2, which is important for achieving good performance of Li-S batteries [35].

The phase evolution was evaluated by X-ray diffraction (XRD) analysis after heat-treatment and sulfur incorporation in Fig. 3(a) and (b), respectively. As shown in Fig. 3(a), there is a very broad peak around 20° in the XRD pattern of MH-SiO_2 annealed at 500 °C for 2 h under Ar, indicating that the MH-SiO_2 is still amorphous after being annealed at 500 °C. For the MH-SiO_2@TiO_2 sample annealed at 500 °C for 2 h under Ar, only anatase TiO_2 (JCPDS No. 78-2486) can be detected. However, with the sintering temperature increased to 800 °C, the position and intensity of the peaks are well matched to the PDF card of hexagonal SiO_2 (JCPDS No. 89-8936), suggesting that SiO_2 turns crystalline at such temperature. Due to the much lower amount of TiO_2 compared to SiO_2, we can hardly find any obvious peak related to it. In addition, the presence of amorphous carbon indicates that 800 °C is a proper temperature for the carbonization of surfactants resulting in improving the electronic conductivity. Furthermore, the XRD patterns of both samples annealed at 500 °C and 800 °C after sulfur incorporation reveal the presence of orthorhombic sulfur (JCPDS No. 08-0247) which is identical to the element sulfur powder (Fig. 3b). To further investigate the structure of MH-SiO_2@TiO_2 samples before and after sulfur infiltration, nitrogen adsorption-desorption isotherms and pore size distribution curves are presented in Fig. 3(c). High surface area with the type IV hysteresis is revealed obviously in Fig. 3(c) with a maximum pore size distribution peak at 2.2 nm (the inset in Fig. 3(c)), demonstrating the presence of huge amount of mesopores in the MH-SiO_2@TiO_2 sample which is consistent with the TEM observation. Such mesopores in the host materials could effectively mitigate the LiPS

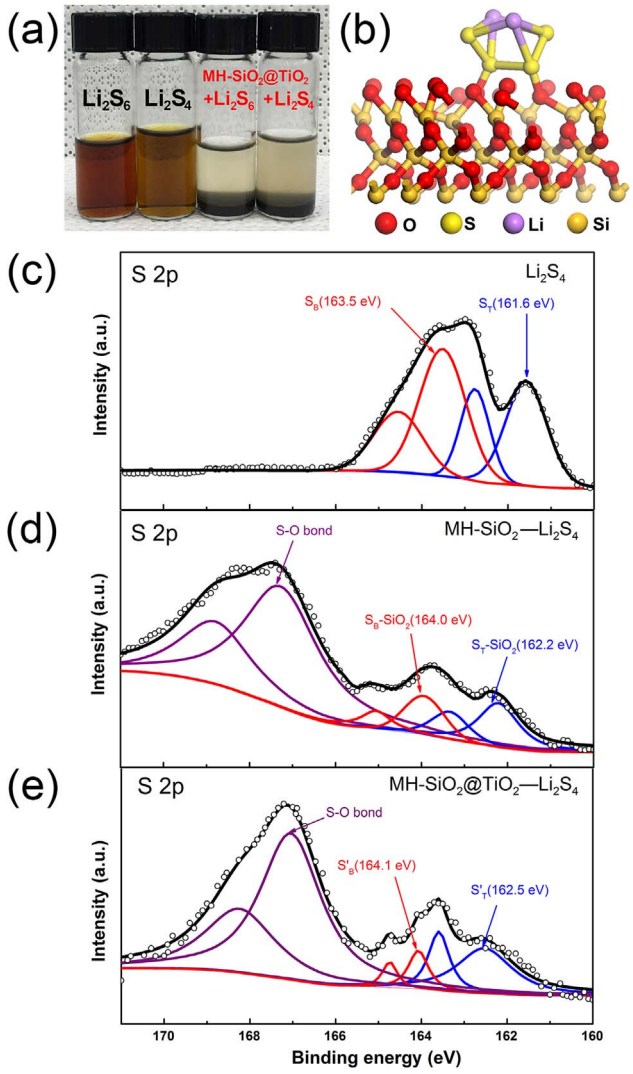

Fig. 4. Illustration of the adsorption of LiPS by MH-SiO_2@TiO_2. (a) Visual discrimination of the Li_2S_6, Li_2S_4 solution before and after MH-SiO_2@TiO_2 addition; (b) The schematic structural model of Li_2S_4 adsorbed on SiO_2 surface with dangling oxygen atoms. The red, orange, yellow and purple balls represent oxygen, silicon, sulfur and lithium atoms, respectively. (c)~(e) XPS spectra of S 2p for Li_2S_4, MH-SiO_2—Li_2S_4 and MH-SiO_2@TiO_2—Li_2S_4, respectively.

dissolution for better cycle retention [9]. In addition, the surface area greatly decreases after sulfur impregnation, providing us with further evidence that sulfur can be filled in the porous hosts. By performing the thermogravimetric analysis (TGA) from room temperature to 800 °C at a heating rate of 10 °C/min under N_2 atmosphere (Fig. 3(d)), the sulfur content in the MH-SiO_2@TiO_2/S composite is determined to be as high as 80 wt%. It is worth noting that there have been only a few reports [20,24] demonstrating such high sulfur loading.

The interaction of different LiPS (Li_2S_6 and Li_2S_4) with our host material was probed using a combination of visual discrimination, XPS and first-principles calculations. As shown in Fig. 4(a), the superior LiPS adsorption capability of MH-SiO_2@TiO_2 can be revealed very apparently by the immediate discoloration by the addition of vacuum dried MH-SiO_2@TiO_2 powder into Li_2S_6 and Li_2S_4 solutions. Furthermore, XPS was performed using Li_2S_4 as the representative LiPS to study the interaction. XPS spectra (S 2p) of Li_2S_4, Li_2S_4-MH-SiO_2 and Li_2S_4-MH-SiO_2@TiO_2 were collected after vacuum drying the corresponding mixture solutions, as demonstrated in Fig. 4(c), (d) and (e), respectively. Herein we only quote the $2p_{3/2}$ component of the $2p_{3/2}/2p_{1/2}$ doublets. The characteristic peaks of Li_2S_4 in Fig. 4(c) at 161.6 eV and 163.5 eV are assigned to the terminal (S_T) and bridging sulfur (S_B) [17], respectively. Although SiO_2 has been revealed as an effective LiPS reservoir material [23,31–33], the precise mechanism of the interaction between LiPS and SiO_2 is rarely reported. To address this issue, we performed XPS also on Li_2S_4-MH-SiO_2, as shown in Fig. 4(d). On the one hand, the peaks at 164.0 eV (S_B-SiO_2) and 162.2 eV (S_T-SiO_2) exhibit a +0.5 eV and +0.6 eV shift compared to S_B and S_T in Li_2S_4, respectively. On the other hand, the formation of S–O bond [36,37] can be clearly identified by the strong wide peak in the range of 165–170 eV. In addition, we speculate that the small peak at 160.7 eV is attributed to the interaction of Si with S. There were some studies that show possible reaction between silicon and sulfur [38–40]. Such results reveal a strong interaction between polysulfide species and SiO_2. Similar strong interaction can also be revealed by the spectrum of Li_2S_4-MH-SiO_2@TiO_2 shown in Fig. 4(e). Since the thickness of TiO_2 (~10 nm) on the MH-SiO_2 surface is very close to the penetration depth of X-rays used in XPS, the changed sulfur environment is believed to mainly stem from the interaction between element sulfur and TiO_2. Additionally, for Si 2p (Fig. S4a) and Ti 2p spectra (Fig. S4b), we can also observe a −1.3 eV and −1.1 eV shift to lower binding energy, respectively, illustrating the increased electron density at the metal center [41]. To better understand the adsorption mechanism of Li_2S_4 and SiO_2 surface, different Li_2S_4-SiO_2 surface models have been constructed and studied by first-principles calculations. It was found that Li_2S_4 clusters are easily bonded with the dangling or unsaturated oxygen atoms on the SiO_2 surfaces. A typical schematic structural model of Li_2S_4 adsorbed on SiO_2 surface is shown in Fig. 4(b). The red, orange, yellow and purple balls represent oxygen, silicon, sulfur and lithium atoms, respectively. It is obvious that two sulfur atoms are bonded with two dangling oxygen atoms and form two S–O bonds with calculated bond length of about 1.5 Å. The calculated binding energy is 10.96 eV for the above model, which coincides with the double of S–O bond energy (about 5.4 eV), revealing that covalent S–O bond could indeed be formed between Li_2S_4 and SiO_2 surfaces.

To evaluate the electrochemical properties of MH-SiO_2@TiO_2/S composites, 2032 type coin cells were assembled. The binder is PVDF and the conductive agent is Super C65. The electrolyte/sulfur (E/S) ratio is 13 μL/mg. Fig. 5(a) shows the various charge/discharge voltage profiles of the composite cathode at different current densities ranging from 0.05 C to 1 C (1 C is defined as 1675 mA/g). All the discharge voltage profiles exhibit two typical discharge plateaus corresponding to the reduction from sulfur to the long-chain (~2.3 V) and short-chain LiPS (~2.1 V), respectively. The results of charge/discharge voltage profiles are consistent with the cyclic voltammetry (CV) plots shown in Fig. S5. The increment in the current density only results in a slightly increased polarization, indicative of good kinetics due to the good dispersion of carbon and microstructures facilitating both the electronic conductivity and the accessibility of electrolytes. As shown in Fig. 5(b) regarding the rate performance, the composite electrodes deliver high initial specific capacity of 1271 mAh/g at 0.05 C and stabilized specific capacity of 906, 825 and 797 mAh/g at 0.2 C, 0.5 C and 1 C, respectively. When the current density switches back to 0.5 C 0.2 C and 0.05 C, the discharge capacity can be recovered to their original values at the same current density levels, indicating the reliability and stability of the MH-SiO_2@TiO_2/S composites.

To show the structural advantages of MH-SiO_2@TiO_2 as the sulfur host, two control samples are also prepared. First, S/MH-SiO_2@TiO_2–500 was synthesized by annealing the MH-SiO_2@TiO_2 at 500 °C for 2 h under Ar and then undergoing sulfur impregnation. Although the S/MH-SiO_2@TiO_2–500 delivers an initial specific capacity of 888 mAh/g at a current density of 0.5 C, the capacity retention is only 63.1% after 300 cycles, as shown in Fig. 5(c). Such poor capacity retention is due to the incomplete carbonization of surfactants at 500 °C resulting in insufficient conductivity. The second control sample S/MH-SiO_2–800 was prepared by annealing MH-SiO_2 (without TiO_2 coating) at 800 °C for 2 h under Ar and then undergoing sulfur impregnation. The S/MH-SiO_2–800 sample exhibits even worse capa-

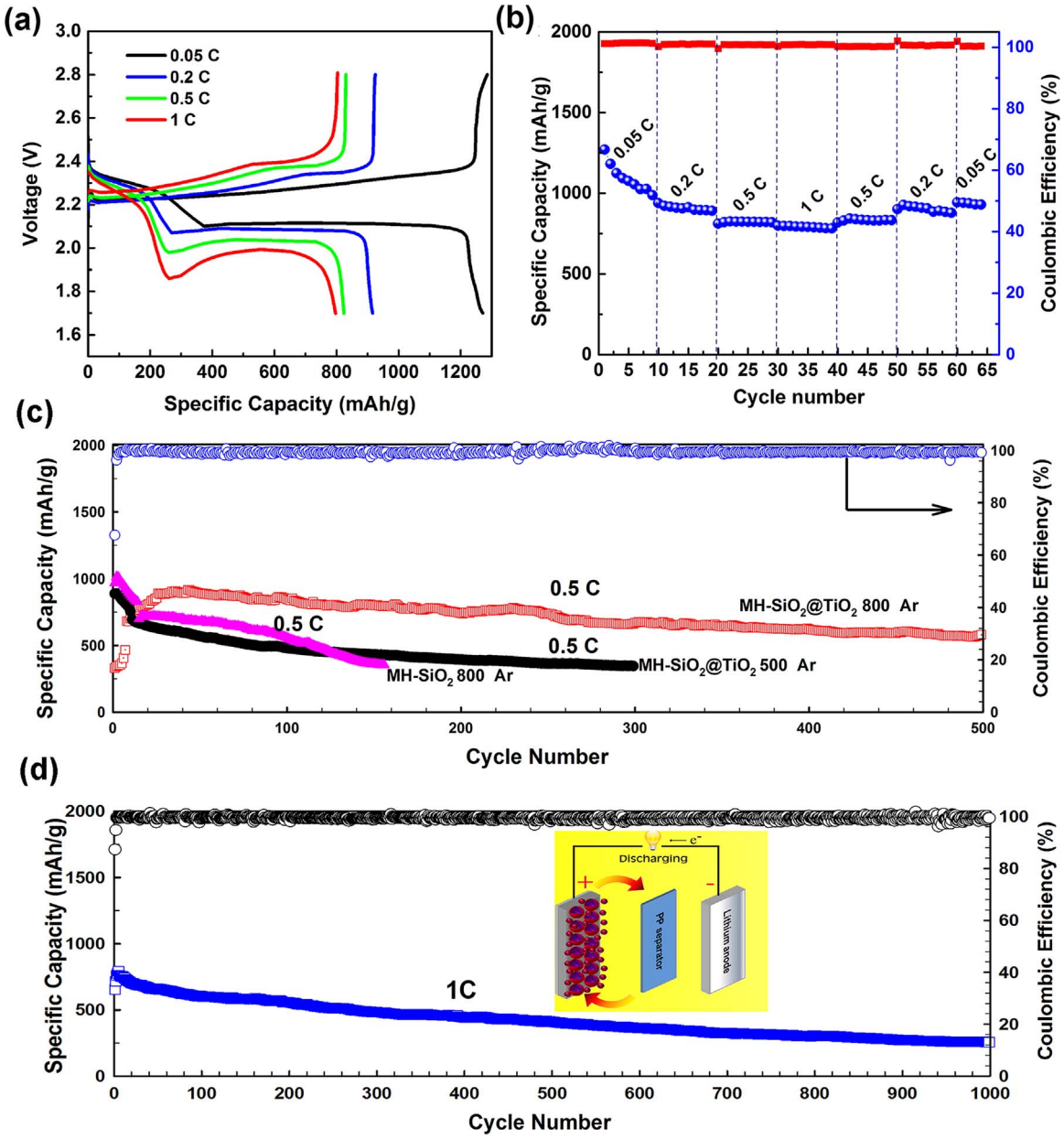

Fig. 5. Electrochemical properties of MH-SiO_2@TiO_2/S composites. (a) Charge and discharge voltage profiles at various densities ranging from 0.05 C to 1 C (1 C=1675 mA/g); (b) Rate performance; (c) Cycling performance and Coulombic efficiency of S composites electrodes at 0.5 C. Host materials including MH-SiO_2@TiO_2 heat-treated at 800 °C and 500 °C for 2 h and MH-SiO_2 heat-treated at 800 °C for 2 h; (d) Long-term cycling performance and Coulombic efficiency of S/ MH-SiO_2@TiO_2 (800 °C, 2 h) composites at high current density of 1 C.

city retention due to the insufficient capability for confining LiPS in the presence of only mesoporous SiO_2 at such high sulfur loading as shown in Fig. 5(c). In comparison, benefiting from its good conductivity and double-oxide microstructure, the S/MH-SiO_2@TiO_2 (annealed at 800 °C for 2 h under Ar) electrode shows a high specific capacity of 916 mAh/g at 0.5 C after activating for ~30 cycles and much better capacity retention of 65.5% over 500 cycles. Furthermore, the long cycle performance of the battery with such composite electrode was measured at a higher rate (1 C) over 1000 cycles, as exhibited in Fig. 5(d). A high specific capacity of 793 mAh/g is achieved with ~33% capacity retention over 1000 cycles, suggesting that the host material with our designed microstructure can effectively mitigate the polysulfide shuttling effect even at a very high sulfur loading of 80 wt%.

To further verify the stability of MH-SiO_2@TiO_2 in cycling, the morphology of the electrode after cycling for 500 cycles at 0.5 C has been examined at fully charged state. Well maintained spherical and mesoporous morphologies after cycling for 500 cycles can be clearly identified by SEM and HRTEM observations in Fig. S6 and Fig. S7(a), respectively, indicating the good mechanical robustness of the host for accommodating the large volume change between S↔Li_2S. As shown in Fig. S7(b) and (c), the TiO_2 coating can also preserve its structural integrity, despite the nano-TiO_2 has turned amorphous after cycling, which is consistent with our previous research [42]. Therefore, we can conclude that the microstructural stability of our sulfur cathode "secondary particle" is excellent, which explains the good cyclability. The EDS mapping images shown in Fig. S8 reveal that the distribution of S is in accordance with that of Si and O demonstrating the favorable adsorption capability of sulfur species by our hosts. Furthermore, EIS plots based on the MH-SiO_2@TiO_2/S and C/S composite (the same sulfur content as MH-SiO_2@TiO_2/S, preparation details in Supplementary Information) electrodes measured in the frequency range from 100 kHz to 100 mHz, were shown in Fig. S9(a). According to the results fitted to an equivalent circuit model, the MH-SiO_2@TiO_2/S electrode exhibits a smaller charge-transfer resistance (R_{ct}) than that

of the C/S electrode both before and after cycling, indicating an enhanced charge-transfer capability in the composite secondary particle. To evaluate dynamics for lithium insertion and extraction, EIS measurements were performed at different depths of discharge (DOD) in the first discharge cycle. It can be seen from Fig. S9 (b) and (c) that the Nyquist plots could be divided into two types. EIS spectra at points A (0% DOD) and B (10% DOD) only exhibit one depressed semi-circle followed by an inclined line; while the EIS spectra at points C (40% DOD), D (70% DOD) and E (100% DOD) present two depressed semi-circles and an inclined line. From A to C, the R_{ct} decreases greatly due to the dissolution of LiPS into liquid electrolytes, suggesting facile kinetics of lithium insertion into the MH-SiO_2@TiO_2/S cathode. From C to E, the resistance from the solid Li_2S_2/Li_2S film (R_L) increases continuously until the end of discharge, owing to the gradual formation of low electrical conductive Li_2S_2/Li_2S films.

3. Conclusion

In summary, we have designed and synthesized an efficient sulfur host based on double oxides constructed from SiO_2 hollow spheres with radial meso-channels which are covered by a thin TiO_2 coating. This novel host can maximize the sulfur loading and effectively confine LiPS for prolonged cycling life by the synergistic effects of such double oxides. Meanwhile, the carbonization of surfactants used in the synthesis process can provide the host with good electrical conductivity to facilitate electron access and hence improve sulfur utilization. Benefitting from the unique structural and compositional advantages, we achieve a high sulfur loading up to 80 wt% with ~65.5% and 33% capacity retentions over 500 and 1000 cycles when tested at 0.5 C and 1 C, respectively. Furthermore, by first-principles calculations and XPS the formation of S–O bond has been revealed to be the dominate adsorption mechanism between LiPS and SiO_2 for the first time.

Acknowledgements

Weijiang Xue and Chang-An Wang are grateful to the support by National Natural Science Foundation of China (51572145) and China Postdoctoral Science Foundation (2015M571037). Authors also would like to acknowledge the support by Samsung Advanced Institute of Technology. This work made use of the MRSEC Shared Experimental Facilities supported by the National Science Foundation under award number DMR-1419807.

Appendix A. Supporting information

Supplementary data associated with this article can be found in the online version at doi:10.1016/j.nanoen.2017.05.041.

References

[1] A. Manthiram, Y. Fu, S.H. Chung, C. Zu, Y.S. Su, Chem. Rev. 114 (2014) 11751–11787.
[2] Q. Pang, X. Liang, C.Y. Kwok, L.F. Nazar, Nat. Energy 1 (2016) 16132.
[3] S. Bai, X. Liu, K. Zhu, S. Wu, H. Zhou, Nat. Energy 1 (2016) 16094.
[4] D. Lv, J. Zheng, Q. Li, X. Xie, S. Ferrara, Z. Nie, L.B. Mehdi, N.D. Browning, J.-G. Zhang, G.L. Graff, J. Liu, J. Xiao, Adv. Energy Mater. 5 (2015) 1402290.
[5] L. Xiao, Y. Cao, J. Xiao, B. Schwenzer, M.H. Engelhard, L.V. Saraf, Z. Nie, G.J. Exarhos, J. Liu, J. Mater. Chem. A 1 (2013) 9517–9526.
[6] C. Zheng, S. Niu, W. Lv, G. Zhou, J. Li, S. Fan, Y. Deng, Z. Pan, B. Li, F. Kang, Q.-H. Yang, Nano Energy 33 (2017) 306–312.
[7] G. Xu, Q.-b. Yan, A. Kushima, X. Zhang, J. Pan, J. Li, Nano Energy 31 (2017) 568–574.
[8] X. Ji, K.T. Lee, L.F. Nazar, Nat. Mater. 8 (2009) 500–506.
[9] Y. Zhao, W. Wu, J. Li, Z. Xu, L. Guan, Adv. Mater. 26 (2014) 5113–5118.
[10] X.-B. Cheng, J.-Q. Huang, Q. Zhang, H.-J. Peng, M.-Q. Zhao, F. Wei, Nano Energy 4 (2014) 65–72.
[11] J. Cao, C. Chen, Q. Zhao, N. Zhang, Q. Lu, X. Wang, Z. Niu, J. Chen, Adv. Mater. 28 (2016) 9629–9636.
[12] C. Wang, X. Wang, Y. Yang, A. Kushima, J. Chen, Y. Huang, J. Li, Nano Lett. 15 (2015) 1796–1802.
[13] C. Zu, A. Manthiram, Adv. Energy Mater. 3 (2013) 1008–1012.
[14] X. Li, Y. Chen, H. Huang, Y.-W. Mai, L. Zhou, Energy Storage Mater. 5 (2016) 58–92.
[15] L. Qie, C. Zu, A. Manthiram, Adv. Energy Mater. 6 (2016) 1502459.
[16] X. Liu, J.Q. Huang, Q. Zhang, L. Mai, Adv. Mater. (2017) 1601759.
[17] X. Liang, C. Hart, Q. Pang, A. Garsuch, T. Weiss, L.F. Nazar, Nat. Commun. 6 (2015) 5682.
[18] Z. Li, J. Zhang, X.W. Lou, Angew. Chem. Int Ed. 54 (2015) 12886–12890.
[19] X. Wang, G. Li, J. Li, Y. Zhang, A. Wook, A. Yu, Z. Chen, Energy Environ. Sci. 9 (2016) 2533–2538.
[20] X. Liang, C.Y. Kwok, F. Lodi-Marzano, Q. Pang, M. Cuisinier, H. Huang, C.J. Hart, D. Houtarde, K. Kaup, H. Sommer, T. Brezesinski, J. Janek, L.F. Nazar, Adv. Energy Mater. 6 (2016) 1501636.
[21] N. Liu, Z. Lu, J. Zhao, M.T. McDowell, H.W. Lee, W. Zhao, Y. Cui, Nat. Nanotechnol. 9 (2014) 187–192.
[22] Z. Wei Seh, W. Li, J.J. Cha, G. Zheng, Y. Yang, M.T. McDowell, P.C. Hsu, Y. Cui, Nat. Commun. 4 (2013) 1331.
[23] S. Rehman, S. Guo, Y. Hou, Adv. Mater. 28 (2016) 3167–3172.
[24] X. Liang, L.F. Nazar, ACS Nano. 10 (2016) 4192–4198.
[25] M.A. Pope, I.A. Aksay, Adv. Energy Mater. 5 (2015) 1500124.
[26] J. Song, M.L. Gordin, T. Xu, S. Chen, Z. Yu, H. Sohn, J. Lu, Y. Ren, Y. Duan, D. Wang, Angew. Chem. Int Ed. 54 (2015) 4325–4329.
[27] Y. Yao, M.T. McDowell, I. Ryu, H. Wu, N. Liu, L. Hu, W.D. Nix, Y. Cui, Nano Lett. 11 (2011) 2949–2954.
[28] H. Kobayashi, M. Hibino, Y. Kubota, Y. Ogasawara, K. Yamaguchi, T. Kudo, S.I. Okuoka, H. Ono, K. Yonehara, Y. Sumida, N. Mizuno, J. Electrochem. Soc. 164 (2017) A750–A753.
[29] G. Xu, Q.B. Yan, S. Wang, A. Kushima, P. Bai, K. Liu, X. Zhang, Z. Tang, J. Li, 2017 (In prepartion).
[30] M.L. Sushko, K.M. Rosso, J. Liu, J. Phys. Chem. Lett. 1 (2010) 1967–1972.
[31] K.T. Lee, R. Black, T. Yim, X. Ji, L.F. Nazar, Adv. Energy Mater. 2 (2012) 1490–1496.
[32] P. Wei, M. Fan, H. Chen, D. Chen, C. Li, K. Shu, C. Lv, Int J. Hydrog. Energy 41 (2016) 1819–1827.
[33] X. Ji, S. Evers, R. Black, L.F. Nazar, Nat. Commun. 2 (2011) 325.
[34] Z. Teng, X. Su, Y. Zheng, J. Sun, G. Chen, C. Tian, J. Wang, H. Li, Y. Zhao, G. Lu, Chem. Mater. 25 (2012) 98–105.
[35] X. Tao, J. Wang, C. Liu, H. Wang, H. Yao, G. Zheng, Z.W. Seh, Q. Cai, W. Li, G. Zhou, C. Zu, Y. Cui, Nat. Commun. 7 (2016) 11203.
[36] X. Tao, J. Wang, Z. Ying, Q. Cai, G. Zheng, Y. Gan, H. Huang, Y. Xia, C. Liang, W. Zhang, Y. Cui, Nano Lett. 14 (2014) 5288–5294.
[37] G. Xu, J. Yuan, X. Tao, B. Ding, H. Dou, X. Yan, Y. Xiao, X. Zhang, Nano Res. 8 (2015) 3066–3074.
[38] A. Haas, Angew. Chem. Int Ed. 4 (1965) 1014–1023.
[39] R. Azhakar, R.S. Ghadwal, H.W. Roesky, R.A. Mata, H. Wolf, R. Herbst-Irmer, D. Stalke, Chem. Eur. J. 19 (2013) 3715–3720.
[40] S.K. Coulter, M.P. Schwartz, R.J. Hamers, J. Phys. Chem. B 105 (2001) 3079–3087.
[41] Q. Pang, D. Kundu, M. Cuisinier, L.F. Nazar, Nat. Commun. 5 (2014) 4759.
[42] S. Li, J. Niu, Y.C. Zhao, K.P. So, C. Wang, C.A. Wang, J. Li, Nat. Commun. 6 (2015) 7872.

Weijiang Xue is now a postdoctoral associate in Prof. Ju Li's group in Department of Nuclear Science and Engineering at Massachusetts Institute of Technology. He obtained his Ph.D degree from Tsinghua University in 2013. His research interests mainly focus on the design and application of advanced energy storage materials in lithium-ion batteries, lithium-sulfur batteries and lithium-air batteries.

Qing-Bo Yan is an associate professor of University of Chinese Academy of Sciences (UCAS) and recently a visiting scholar in Department of Nuclear Science and Engineering at Massachusetts Institute of Technology. His research interest is mainly on the physical properties of two-dimensional materials and energy storage materials through density functional theory based first-principles calculations and other atomistic simulation methods. Dr. Yan obtained his Ph.D. degree in the College of Physical Sciences at UCAS in 2009.

Guiyin Xu received his M.E. degrees in Applied Chemistry from Nanjing University of Aeronautics and Astronautics in 2014. He is currently pursuing his Ph.D. degree under the co-supervision of Prof. Xiaogang Zhang and Prof. Ju Li in Department of Nuclear Science and Engineering at Massachusetts Institute of Technology. His research focuses on advanced electrode materials for energy storage devices, such as supercapacitors, lithium-ion batteries and Li-S batteries.

Liumin Suo received his Ph.D. in condensed matter physics in 2013 at Institute of Physics, Chinese Academy of Sciences (IoP-CAS). He is currently postdoctoral Research Associate at Massachusetts Institute of Technology (MIT). His research interests focus on energy storage devices including electrode materials, electrolyte and electrochemistry for rechargeable batteries (rechargeable aqueous lithium ion batteries, lithium-sulfur batteries and lithium metal batteries).

Yuming Chen received his Ph.D degree from The Hong Kong Polytechnic University in 2014. He is now working as a postdoctoral fellow in Prof. Ju Li's group at MIT. His current research interests include the design and development of nanomaterials and their applications in energy and environment.

Chao Wang is currently a postdoctor in Prof. Ju Li's group at MIT in Department of Nuclear Science and Engineering. She received her Ph.D at Huazhong University of Science and Technology under the co-supervision of Prof. Yunhui Huang and Prof. Jitao Chen in College of Chemistry and Molecular Engineer at Peking University. Her research is mainly focused on advanced electrode materials and additives for energy storage devices, such as Li-S batteries and lithium metal batteries.

Chang-An Wang is now a professor in School of Materials Science and Engineering at Tsinghua University. He was a post-doctor research fellow in School of Materials Science and Engineering at Georgia Institute of Technology, USA. He is an editorial board member of Frontiers of Materials Science, Journal of the Chinese Ceramic Society, and Journal of ceramics. His research is highly focused on advanced ceramics and ceramic matrix composites, especially on porous ceramics in the field of catalysts, supercapacitors and batteries.

Ju Li is BEA Professor of Nuclear Science and Engineering and Professor of Materials Science and Engineering at MIT. His group (http://Li.mit.edu) performs computational and experimental research on mechanical properties of materials, and energy storage and conversion. Ju was a recipient of the 2005 Presidential Early Career Award for Scientists and Engineers, 2006 MRS Outstanding Young Investigator Award, and 2007 TR35 award from *Technology Review* magazine. Ju was elected a Fellow of the American Physical Society in 2014 and a Fellow of the Materials Research Society in 2017.

Supplementary Information for

Double-oxide sulfur host for advanced lithium-sulfur batteries

Weijiang Xue[1,2], Qing-Bo Yan[2,3], Guiyin Xu[2], Liumin Suo[2], Yuming Chen[2], Chao Wang[2], Chang-An Wang[1,*] and Ju Li[2,*]

[1]State Key Lab of New Ceramics and Fine Processing, School of Materials Science and Engineering, Tsinghua University, Beijing 100084, P. R. China.

[2]Department of Nuclear Science and Engineering and Department of Materials Science and Engineering, Massachusetts Institute of Technology, Cambridge, Massachusetts 02139, USA.

[3]College of Materials Science and Opto-Electronic Technology, University of Chinese Academy of Science, Beijing, 100049, P. R. China

[*]Corresponding authors

Email address: wangca@mail.tsinghua.edu.cn (C. A. W); liju@mit.edu (J. L)

1. Experimental procedure

Preparation of MH-SiO_2@TiO_2 and other control materials.

SiO_2 hollow spheres with radial meso-channels (MH-SiO_2) were prepared by a self-assembly method using a surfactant cetyltrimethylammonium bromide (CTAB) as structure-directing agents[1]. Firstly, CTAB was fully dissolved in the mixture of ethanol (EtOH), deionized water (DIW) and concentrated ammonia aqueous solution (28 wt%). The weight ratio of the mixture was 0.16 CTAB: 12 EtOH: 50 DIW: 1 NH_4OH. Then 1mL of tetraethyl orthosilicate (TEOS) was quickly injected into the mixture under vigorous stirring for 24 hr. SiO_2 spheres can be formed during the hydrolysis of TEOS which is assembled with CTAB via electrostatic interaction. It is important to note that at the presence of such high EtOH/DIW ratios and structure-directing agents, a gradient of chemical stability from the core to shell will form. Therefore, the silicate-CTAB composites in the inner part with lower chemical stability are more easily attacked by hot water molecular and hence dissolved first. The M-SiO_2 was subsequently collected by centrifugation and washed for 3 times with DIW and EtOH. Then, the MH-SiO_2 was obtained by re-dispersing the M-SiO_2 in 120 mL DIW and incubated at 70 ^oC for 24~72 hr.

For TiO_2 coating[2], 150 mg fully dried MH-SiO_2 powders were mixed with 30 mL EtOH, 0.3 mL DIW and 50 mg hydroxypropyl cellulose (HPC) under vigorous stirring. Tetrabutylorthotitanate [$Ti(OC_4H_9)_4$, TBOT] dissolved in 5 mL EtOH was injected into the mixture and then heated at 85 ^oC for 90 min under reflux. The powders were collected by

washing with DIW and ethanol for 3 times and dried at 60 °C for 12 hr. For sulfur host materials, MH-SiO_2@TiO_2 and control samples MH-SiO_2 were obtained by annealing at 500 °C ~800 °C under Ar atmosphere for 2 hr.

Preparation of MH-SiO_2@TiO_2/S composites and other control materials.

For sulfur incorporating into the host materials, a traditional melt-diffusion method was conducted[3]. The mixture of MH-SiO_2@TiO_2 and commercial sulfur powder with a ratio of 1:4 (weight ratio) was sealed in a hydrothermal reactor under Ar protection and heated at 155 °C for 12 hr. After cooling down to room temperature, MH-SiO_2@TiO_2/S was obtained. The same method was used in the preparation of other control samples. C/S composite was fabricated using Super C65 and commercial sulfur powder with a ratio of 1:4 (weight ratio).

LiPSs absorption study and preparation of XPS samples.

Li_2S_8, Li_2S_6 and Li_2S_4 solutions were synthesized by reacting lithium sulfide (Li_2S) and elemental sulfur in the desired ratio[4] in anhydrous dimethoxyethane (DME) solvent[5] in an Ar-filled glovebox. For LiPS absorption study, 30 mg of MH-SiO_2@TiO_2 was added into two glass vials. Subsequently, about 3 mL of Li_2S_8 and Li_2S_6 solutions were added. Two blank vials were also filled with the same Li_2S_8 and Li_2S_6 solutions as control samples, respectively.

For XPS sample, Li_2S_4 solution was mixed with MH-SiO_2 and MH-SiO_2@TiO_2 powder under vigorous stirring for 2 hr and settled for several minutes. Then the supernatant was removed and XPS samples were obtained by drying the precipitates under vacuum.

First-principles calculations.

The calculations were performed using Vienna ab initio simulation package (VASP)[6], which was based on density functional theory (DFT)[7] and the projected augmented wave (PAW) method[8]. Generalized gradient approximation (GGA) in the form of Perdew-Burke-Ernzerhof (PBE)[9] was used for the exchange correlation potential. The DFT-TS method[10] was adopted to take into account the van der Waals interactions. The kinetic energy cutoff for plane wave functions was set to 500 eV. All structures were optimized and the maximum force on each atom was less than 0.02 eV $Å^{-1}$. Supercells containing three SiO atomic layers (the bottom layer was fixed during optimization) and a vacuum spacing larger than 15 Å was used to model the SiO_2 (001) surface. The binding energies (E_b) are defined as the difference between the total energy (E_{tot}) of

Li_2S_4-surface adsorption systems, and the energy sum of Li_2S_4 and SiO_2 surface:

$$E_b = \left(E_{Li_2S_4} + E_{surface}\right) - E_{tot}$$

Characterization.

The characterization of microstructures was conducted by scanning electron microscope (Zeiss Merlin High-resolution SEM) and Transmission Electron Microscopy (TEM, Technai G2) at 200 kV. Mapping scanning of various elements was recorded by EDS spectroscopy attached to the Technai G2 TEM. Phase composition was characterized by X-ray diffraction (XRD, Panalytical Multipurpose Diffractometer). Nitrogen adsorption-desorption isotherms analysis was done by NOVA 4000 automated gas sorption system. The sulfur content in cathode composite powder was determined by Thermogravimetric analyses (TG-DSC, SDT Q600) under Nitrogen protection. The elemental and chemical spectroscopic analysis was performed by X-ray photoelectron spectra (XPS, aka ESCA). For XPS, the samples were transferred to the ultra-high vacuum chamber using a specific transfer vessel to avoid contact with air. The values of binding energy were calibrated by using 285.0 eV of C 1s peak.

Electrochemical measurements.

The working electrode was fabricated by mixing 80 wt% of MH-SiO_2@TiO_2/S (1:4 weight ratio) powder, 10 wt% of conductive carbon (Super C65) and 10 wt% of PVDF for 24 hr and then the homogeneous slurry was cast onto an aluminum foil. The control sample of C/S electrode was fabricated using the same method. All the electrodes were dried at 60 °C in an oven for 12 hr and then rolled and cut into round disks. The areal mass loading of the above cathodes is about 1.6~2 mg/cm^2 and the electrode thickness is ~55 um. 2032 type coin cells were assembled using Celgard 2300 separators and metal Li as anode in Ar-filled glove box. The electrolyte was 1.85 M lithium bis (trifluoromethanesulfonyl) imide (LiTFSI) in a 1, 3-dioxolane (DOL) and DME mixture (1:1, v/v) with 2 wt% $LiNO_3$. The cells were galvanostatically charged and discharged between 1.7 V and 2.8 V at various C rates (1C=1.675 mA/mg) using a Landt CT 2001A battery cycler. Cyclic voltammetry (CV) and electrochemical impedance spectroscopy (EIS) measurements were performed on an electrochemical workstation (Gamry Instruments, Reference 3000).

References

1. Teng, Z.; Su, X.; Zheng, Y.; Sun, J.; Chen, G.; Tian, C.; Wang, J.; Li, H.; Zhao, Y.; Lu, G. *Chemistry of Materials* **2012,** 25, (1), 98-105.
2. Fang, S.; Shen, L.; Xu, G.; Nie, P.; Wang, J.; Dou, H.; Zhang, X. *ACS applied materials & interfaces* **2014,** 6, (9), 6497-503.
3. Manthiram, A.; Fu, Y.; Chung, S. H.; Zu, C.; Su, Y. S. *Chemical reviews* **2014,** 114, (23), 11751-87.
4. Zhou, G.; Zhao, Y.; Zu, C.; Manthiram, A. *Nano Energy* **2015,** 12, 240-249.
5. Li, Z.; Zhang, J.; Lou, X. W. *Angewandte Chemie* **2015,** 54, (44), 12886-90.
6. Kresse, G.; Furthmüller, J. *Physical review B* **1996,** 54, (16), 11169.
7. Hohenberg, P.; Kohn, W. *Physical review* **1964,** 136, (3B), B864.
8. Kresse, G.; Joubert, D. *Physical Review B* **1999,** 59, (3), 1758.
9. Perdew, J. P.; Burke, K.; Ernzerhof, M. *Physical review letters* **1996,** 77, (18), 3865.
10. Tkatchenko, A.; Scheffler, M. *Physical review letters* **2009,** 102, (7), 073005.

2. Figures

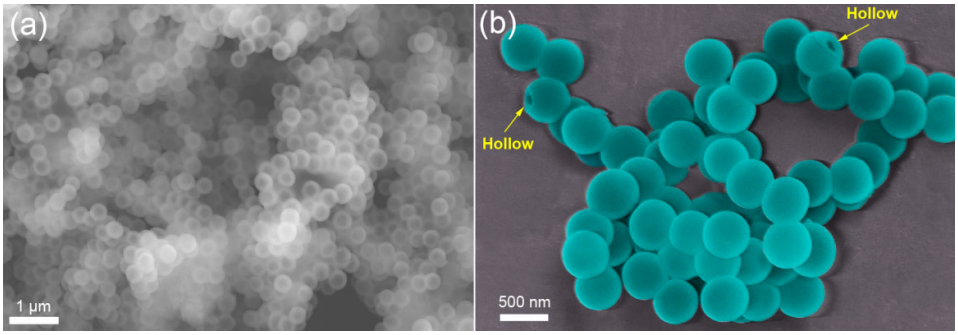

Fig. S1 SEM image of MH-SiO_2 before (a) and after TiO_2 coating (b)

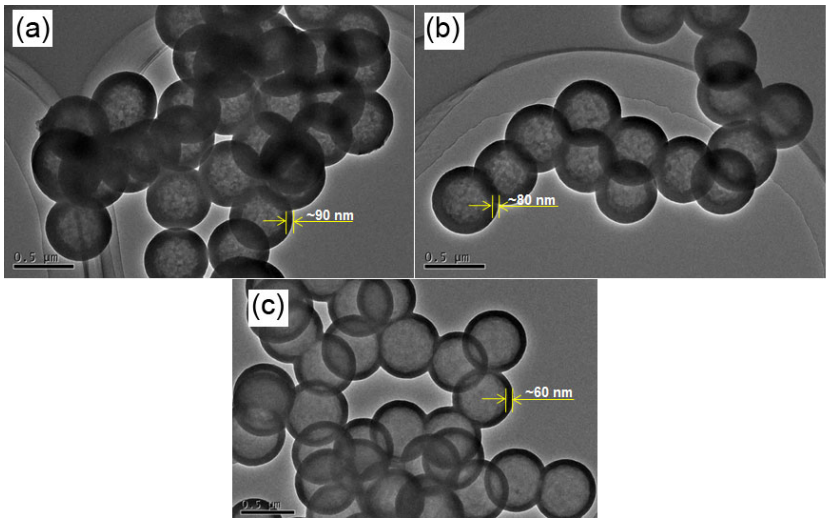

Fig. S2 TEM micrographs of MH-SiO_2 samples showing the shell thickness can be adjusted by the incubation time of 24 hr (a), 48 hr (b) and 72 hr (c) in hot water

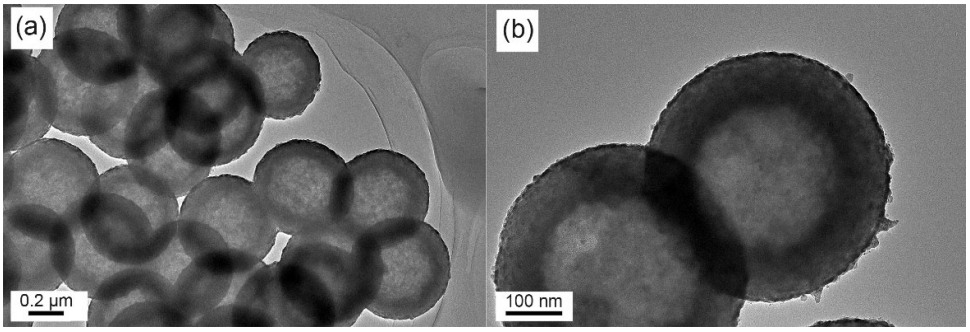

Fig. S3 TEM micrographs of MH-SiO_2@TiO_2 samples demonstrating the uniform TiO_2 coating on the surface of SiO_2 spheres

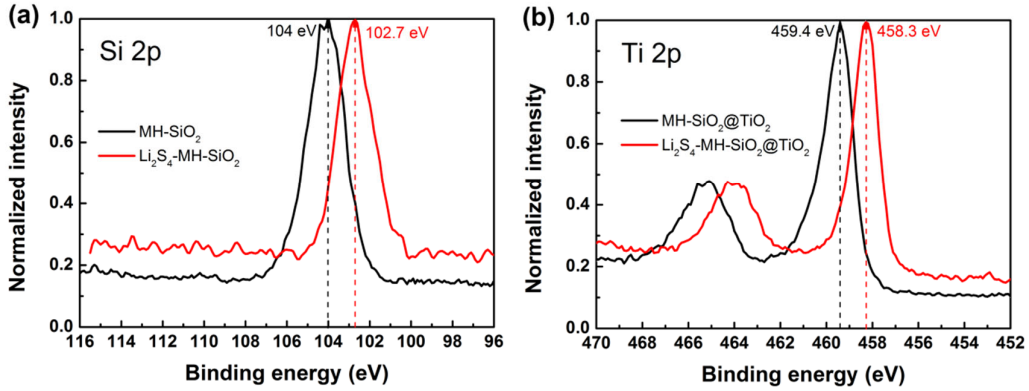

Fig. S4 XPS spectra of Si 2p (a) and Ti 2p (b) of MH-SiO_2 and MH-SiO_2@TiO_2 before and after mixing with Li_2S_4, respectively

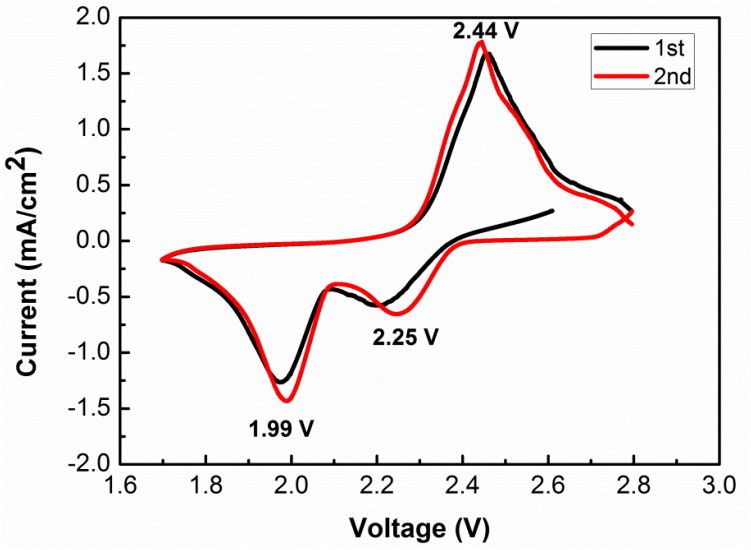

Fig. S5 Cyclic voltammetry (CV) plots of MH-SiO_2@TiO_2/S composite electrode

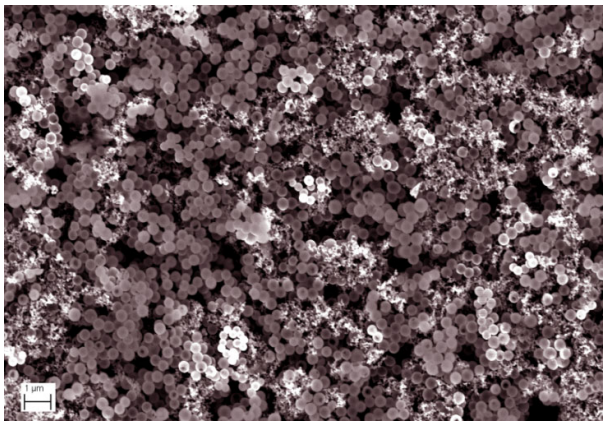

Fig. S6 SEM micrograph of MH-SiO_2@TiO_2/S electrode after cycling for 500 cycles at 0.5 C at fully charged status

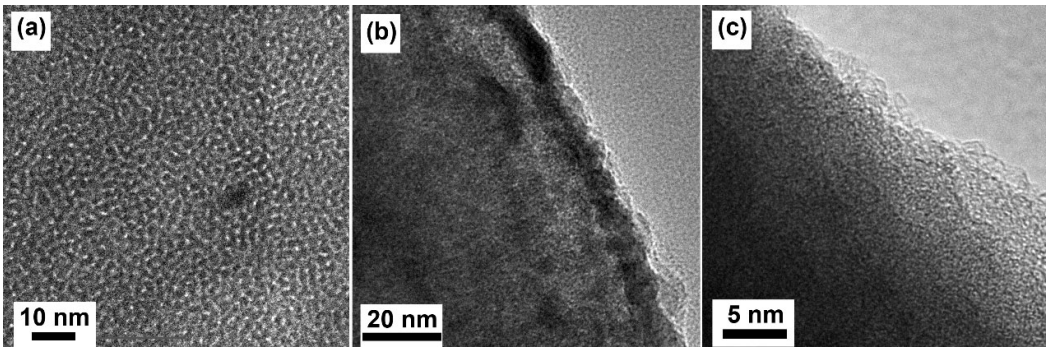

Fig. S7 HRTEM micrographs of MH-SiO_2@TiO_2 host materials after 500 cycles at 0.5 C (a) The well maintained mesoporous morphology of SiO_2; (b) the interface between SiO_2 and TiO_2; (c) the morphology of TiO_2

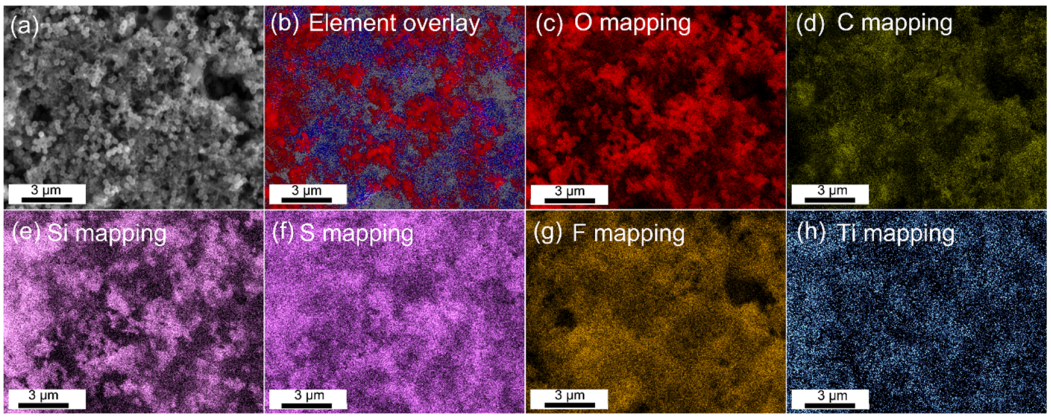

Fig. S8 EDS mapping of MH-SiO_2@TiO_2/S electrode after cycling for 500 cycles at 0.5 C at fully charged state

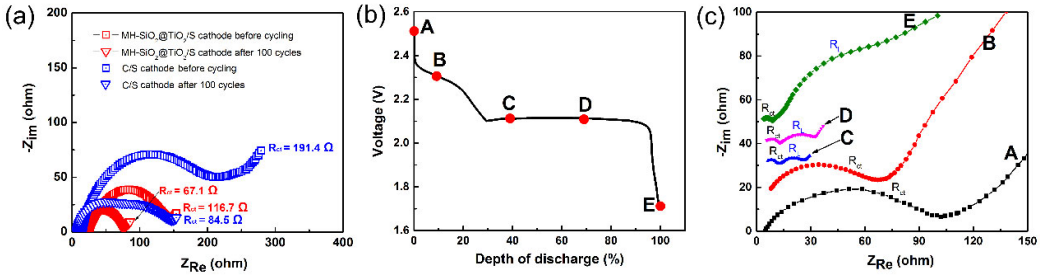

Fig. S9 EIS characterization. (a) EIS spectra of the MH-SiO_2@TiO_2/S and C/S composite electrodes before and after cycling; (b) Voltage profile during the first discharge cycle; (c) EIS spectra at different depths of discharge (DOD) corresponding to (b)